# M$\chi$D candidate nucleus $^{105}$Rh in relativistic mean-field approach

Jian Li and S. Q. Zhang

*School of Physics, State Key Laboratory of Nuclear Physics and Technology, Peking University, Beijing 100871, China*

J. Meng*

*School of Physics and Nuclear Energy Engineering, Beihang University, Beijing 100191, China*

*School of Physics, State Key Laboratory of Nuclear Physics and Technology, Peking University, Beijing 100871, China and*

*Department of Physics, University of Stellenbosch, Stellenbosch, South Africa*

(Dated: January 18, 2013)



## Abstract

Following the reports of two pairs of chiral doublet bands observed in $^{105}$Rh, the adiabatic and configuration-fixed constrained triaxial relativistic mean-field (RMF) calculations are performed to investigate their triaxial deformations with the corresponding configuration and the possible multiple chiral doublet (M$\chi$D) phenomenon. The existence of M$\chi$D phenomenon in $^{105}$Rh is highly expected.

PACS numbers: 21.10.Dr, 21.60.Jz, 21.30.Fe, 27.60.+j

*Electronic address: mengj@pku.edu.cn

Chirality is a topic of general interest in nature science, such as chemistry, biology and physics. The occurrence of chirality in atomic nuclear structure was suggested for triaxially deformed nuclei in 1997 [1] and the predicted patterns of spectra exhibiting chirality — chiral doublet bands — were experimentally observed in 2001 [2]. In addition to the triaxial deformation, the configuration with high-$j$ valence particle(s) and valence hole(s) is also essential for chirality in nuclei. Up to now, candidate chiral doublet bands have been proposed in a number of odd-odd, odd-A or even-even nuclei in the $A \sim 100, 130, 190$ mass regions, for a review, see e.g. [3, 4].

Theory wise, chiral doublet bands were first investigated in the one-particle-one-hole-rotor model (PRM) and the corresponding tilted axis cranking (TAC) approximation [1]. Later on, numerous efforts have been devoted to the development of TAC [5–7] and PRM models [8–12] to describe chiral rotation in atomic nuclei.

RMF theory has received wide attention due to its massive success in describing nuclear global properties and exotic phenomena [13–15]. In order to describe the nuclear rotation phenomena, the cranked RMF theory in the context of principal axis rotation [16, 17] as well as three-dimensional rotation [18] were developed. However due to numerical complexity, it was restricted to two-dimensional studies only, i.e., the magnetic rotation [18, 19].

Based on the adiabatic and configuration-fixed constrained triaxial RMF calculation, triaxial shape coexistence with high-$j$ proton hole- and neutron particle-configurations, are found in $^{106}$Rh, which suggests the existence of a new phenomenon — M$\chi$D [20]. This prediction holds true for other rhodium isotopes $^{104,106,108,110}$Rh as well [21]. In particular, the prediction of the M$\chi$D in $^{106}$Rh remains even with the time-odd fields inclued [22].

Recently, two pairs of chiral doublet bands have been respectively observed in $^{105}$Rh with three-quasiparticle configurations $\pi g_{9/2} \otimes \nu h_{11/2}(g_{7/2}, d_{5/2})$ [23] and $\pi g_{9/2} \otimes \nu h^2_{11/2}$ [24]. It is interesting to verify whether these observations are the predicted M$\chi$D or not in the configuration-fixed constrained triaxial RMF approach. Similar as in Ref. [22], the time-odd fields are included.

The starting point of the RMF theory is the standard effective Lagrangian density constructed with the degrees of freedom associated with nucleon field ($\psi$), two isoscalar meson fields ($\sigma$ and $\omega_\mu$), isovector meson field ($\vec{\rho}_\mu$) and photon field ($A_\mu$) [13–15]. Under "mean-field" and "no-sea" approximations, one can derive the corresponding energy density functional, from which one finds immediately the equation of motion for a single-nucleon

orbital $\psi_i(\boldsymbol{r})$ by variational principle,

$$\{\alpha \cdot [\boldsymbol{p} - \boldsymbol{V}(\boldsymbol{r})] + \beta M^*(\boldsymbol{r}) + V_0(\boldsymbol{r})\}\psi_i(\boldsymbol{r}) = \epsilon_i \psi_i(\boldsymbol{r}), \tag{1}$$

where $M^*(\boldsymbol{r}) \equiv M + g_\sigma \sigma(\boldsymbol{r})$, $M$ the mass of bare nucleon, $V_0(\boldsymbol{r})$ the time-like component of vector potential, and $\boldsymbol{V}(\boldsymbol{r})$ the space-like components of vector fields. The details about the solution of Dirac equation (1) with time-odd fields can be found in Refs. [25, 26].

In the configuration-fixed constrained calculation, the same configuration is guaranteed during the procedure of constraint calculation with the help of "parallel-transport" [27]. In addition to the $\beta^2$-constrained calculation [20], the constraints on the axial and triaxial mass quadrupole moments are also performed to obtained the potential energy surfaces (PES) in the two-dimensional $\beta$-$\gamma$ plane [28].

In the present calculations, each Dirac spinor $\psi_i(\boldsymbol{r})$ is expanded in terms of a set of three-dimensional harmonic oscillator (HO) basis in Cartesian coordinates with 12 major shells and the meson fields with 10 major shells. The pairing correlations are quenched by the unpaired valence nucleons in $^{105}$Rh and thus neglected here. The effective interaction parameter set PK1 [29] is applied. The center-of-mass (c.m.) correction [29, 30] is taken into account by

$$E_{\text{c.m.}}^{\text{mic.}} = -\frac{1}{2MA}\langle \hat{\mathbf{P}}_{\text{c.m.}}^2 \rangle, \tag{2}$$

where $\hat{\mathbf{P}}_{\text{c.m.}}$ is the total momentum operator of a nucleus with mass number $A$. In order to save time, the constrained triaxial RMF calculations without the time-odd fields are performed to search for the triaxial deformation parameters and the valence nucleons configuration favorable for chirality, which will be later confirmed by the calculations with time-odd fields.

The potential energy surface in the $\beta$-$\gamma$ plane ($0 \leqslant \gamma \leqslant 60^\circ$) for $^{105}$Rh in the adiabatic constrained triaxial RMF calculations with PK1 is shown in Fig. 1. All energies are normalized with respect to the binding energy of the absolute minimum, and the contours join points on the surface with the same energy (in MeV). The energy separation between contour lines is 0.4 MeV. From Fig. 1, it shows that the ground state of $^{105}$Rh is triaxially deformed with $\beta = 0.28$ and $\gamma = 23^\circ$. The second minimum is located at the area with $\beta \approx 0.4$ and $\gamma \approx 5^\circ$. The energy difference between these two minima is about 0.5 MeV and corresponding barrier height is about 1.5 MeV. The behavior of shape coexistence is clearly shown.

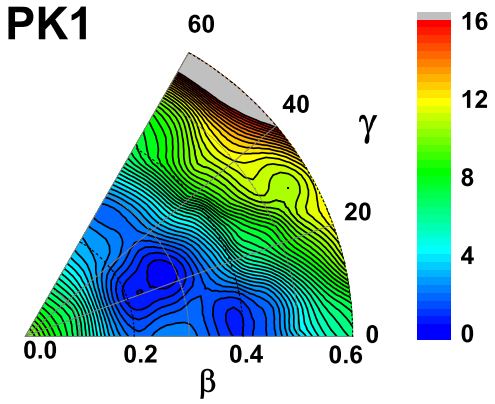


FIG. 1: (Color online) Contour plots of potential energy surface in $\beta$-$\gamma$ plane ($0 \leqslant \gamma \leqslant 60^\circ$) for $^{105}$Rh in constrained triaxial RMF calculations with effective interactions PK1 [29]. All energies are normalized with respect to the binding energy of the absolute minimum (in MeV). The energy separation between contour lines is 0.4 MeV.

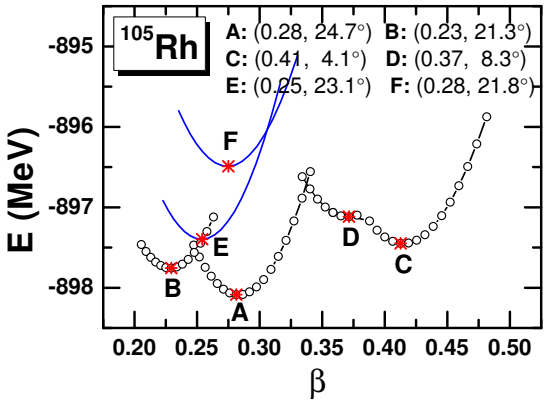


FIG. 2: (Color online) The energy surfaces in adiabatic (open circles) and configuration-fixed (solid lines) constrained triaxial RMF calculation using effective interaction PK1 for $^{105}$Rh. The minima in the energy surfaces for fixed configuration are represented as stars and labeled respectively as A, B, C, D, E, and F. Their corresponding triaxial deformation parameters $\beta$ and $\gamma$ are also given.

The $\beta^2$-constrained calculations, in which the triaxial deformation $\gamma$ is automatically obtained by minimizing the energy, have also been performed. In Fig. 2, the potential energy surfaces as a function of $\beta$ in adiabatic (open circles) constrained triaxial RMF calculation with PK1 for $^{105}$Rh are given, where four minima observed in the potential energy surfaces are labeled with A, B, C, and D respectively.

TABLE I: The total energies $E_{\rm tot}$, triaxial deformation parameters $\beta, \gamma$ as well as their corresponding valence nucleon configurations of minima for A-F in the configuration-fixed constrained triaxial RMF calculations.

| State | Configuration | | $E_{\rm tot}$ | $\beta$ | $\gamma$ |
|---|---|---|---|---|---|
| | Valence nucleons | Unpaired nucleons | | | |
| A | $\pi 1g_{9/2}^{-3} \otimes \nu 1h_{11/2}^{2}$ | $\pi 1g_{9/2}^{-1}$ | -898.09 | 0.28 | 24.7° |
| B | $\pi 1g_{9/2}^{-3} \otimes \nu(1g_{7/2}^{-2}2d_{5/2}^{4})$ | $\pi 1g_{9/2}^{-1}$ | -897.76 | 0.23 | 21.3° |
| C | $\pi(1g_{9/2}^{-4}2p_{3/2}^{-1}1g_{7/2}^{2}) \otimes \nu(1g_{7/2}^{-2}3s_{1/2}^{2}1h_{11/2}^{2})$ | $\pi 2p_{3/2}^{-1}$ | -897.45 | 0.41 | 4.1° |
| D | $\pi(1g_{9/2}^{-4}1g_{7/2}^{1}) \otimes \nu(1g_{7/2}^{-2}1h_{11/2}^{4})$ | $\pi 1g_{7/2}^{1}$ | -897.12 | 0.37 | 8.3° |
| E | $\pi 1g_{9/2}^{-3} \otimes \nu(1h_{11/2}^{1}2d_{5/2}^{1})$ | $\pi 1g_{9/2}^{-1} \otimes \nu(1h_{11/2}^{1}2d_{5/2}^{1})$ | -897.40 | 0.25 | 23.1° |
| F | $\pi 1g_{9/2}^{-3} \otimes \nu(1h_{11/2}^{1}1h_{11/2}^{1})$ | $\pi 1g_{9/2}^{-1} \otimes \nu(1h_{11/2}^{1}1h_{11/2}^{1})$ | -896.40 | 0.28 | 21.8° |

The total energies $E_{\rm tot}$, triaxial deformation parameters $\beta, \gamma$ as well as their corresponding configurations of minima for A-D in the constrained triaxial RMF calculations are presented in Table I. Here, the state A represents the ground state, with triaxial deformation $\beta = 0.28$, $\gamma = 24.7°$ and the corresponding valence nucleon configuration $\pi 1g_{9/2}^{-3} \otimes \nu 1h_{11/2}^{2}$. Note that the two of three proton holes in $1g_{9/2}$ orbital and two neutrons in the $1h_{11/2}$ orbital are pairwise, i.e., they occupy the degenerate time-reversal conjugate levels and don't contribute to the angular momentum. The corresponding unpaired nucleon configuration is $\pi 1g_{9/2}^{-1}$. For state B, the triaxial deformation parameter is ($\beta = 0.23$, $\gamma = 21.3°$), with corresponding valence nucleon configuration $\pi 1g_{9/2}^{-3} \otimes \nu(1g_{7/2}^{-2}2d_{5/2}^{4})$ and unpaired nucleon configuration $\pi 1g_{9/2}^{-1}$. Although A and B have different valence nucleon configurations, they have the same unpaired nucleon configuration.

The triaxial deformation parameters for excited state C and D are ($\beta = 0.41$, $\gamma = 8.3°$) and ($\beta = 0.37$, $\gamma = 8.3°$), respectively. The valence nucleon configuration for C is $\pi(1g_{9/2}^{-4}2p_{3/2}^{-1}1g_{7/2}^{2}) \otimes \nu(1g_{7/2}^{-2}3s_{1/2}^{2}1h_{11/2}^{2})$ and for D $\pi(1g_{9/2}^{-4}1g_{7/2}^{1}) \otimes \nu(1g_{7/2}^{-2}1h_{11/2}^{4})$, while the unpaired nucleon configuration $\pi 2p_{3/2}^{-1}$ for C and $\pi 1g_{7/2}^{1}$ for D. The quadrupole deformations of states C and D are larger than states A and B, which is due to the deformation driving orbital $\pi 1g_{7/2}$ in states C and D. It should be pointed out that states A, B, C and D don't have the suitable particle-hole configurations for chirality.

In the Refs. [23, 24], the observed partners bands with the configurations $\pi 1g_{9/2}^{-1} \otimes$

$\nu 1h^1_{11/2}(1g_{7/2}, 2d_{5/2})^1$ and $\pi 1g^{-1}_{9/2} \otimes \nu(1h^1_{11/2}1h^1_{11/2})$ are respectively suggested as candidate chiral doublet bands. It is interesting to examine the triaxial deformation of these states. For this purpose, the configuration-fixed constrained calculation with the suggested configurations are performed and their corresponding energy surfaces are given in Fig. 2 in blue solid lines, and the energies, configurations and triaxial deformation parameters are listed in Table I. The excitation energy for minima E is 0.69 MeV and for F 1.69 MeV. Furthermore, the triaxial deformation suitable for chirality is found for E and F, namely 23.1° and 21.8° respectively, which together with the corresponding high-$j$ proton hole and high-$j$ neutron particle configurations will lead to the M$\chi$D phenomenon [20]. It should be noted that the present RMF calculations are restricted to the non-rotating mean field only, while the TAC calculations with Woods–Saxon potentials have demonstrated that the rotating mean field will become chiral for configuration E at $\hbar\omega = 0.20$ MeV (strong paring) [23] and for configuration F at $\hbar\omega = 0.60$ MeV (zero pairing) or 0.45 MeV (strong paring) [24]. Recently, the doublet bands with configuration F in $^{105}$Rh are also investigated by triaxial PRM calculations and the evolution of the chiral geometry with angular momentum is discussed [31].

The neutron and proton single-particle levels as functions of deformation $\beta$ are given in Fig. 3, obtained in the adiabatic constrained triaxial RMF calculations for the region $0.247 < \beta < 0.315$. The occupations of neutron and proton for A, E and F are given in Fig. 3(a) and Fig. 3(b) respectively. The single-particle levels with positive (negative) parity are marked by solid (dashed) lines, and occupations are represented by filled circles (two particles) and stars (one particle). It should be pointed out that every single-particle level is degenerated with opposite simplex quantum number [19]. It is easy to see that for ground state A, one valence proton occupies the $1g_{9/2}$ orbit and the last two neutrons occupy the degenerated time reversal conjugate orbit $1h_{11/2}$. For the positive parity state F, the two $1h_{11/2}$ neutrons are unpaired (in contrast to the state A), i.e., they occupy two different $1h_{11/2}$ levels. For the negative parity state E, the two unpaired neutrons occupy the $1h_{11/2}$ and $2d_{5/2}$ levels. It is interesting to note that states E and F compete with each other in energy. However, due to different parities, states E and F do not mix up and could contribute the M$\chi$D phenomenon [20].

Similar as in Ref. [22], the calculations with time-odd fields are also performed to confirm the above discussions. In Table II, the calculated triaxial deformation parameters $\beta, \gamma$, total

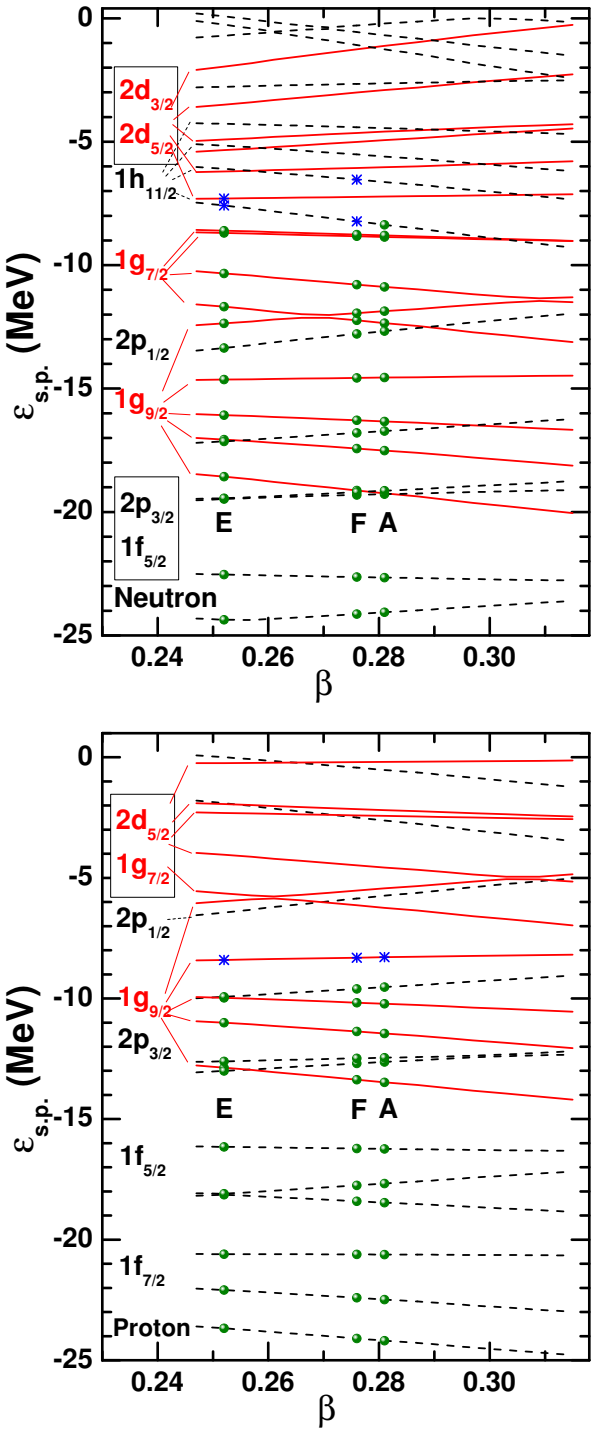


FIG. 3: (Color online) Neutron and proton single-particle levels obtained in constrained triaxial RMF calculations with PK1 as functions of deformation $\beta$. Positive (negative) parity states are marked by solid (dashed) lines. Occupations corresponding to the minima in Fig. 2 are represented by filled circles (two particles) and stars (one particle).

TABLE II: The triaxial deformation parameters $\beta, \gamma$, total energies $E_{\rm tot}$ and the excitation energies $E_{\rm x}$ for states E and F calculated with and without time-odd fields, compared with the experimental bandhead energies of two rotational bands based on the configurations of E and F. The spin and parity $I^\pi$ for ground state and band head of two rotational bands are also given.

| State | Time-even | | Time-odd | | exp | |
|---|---|---|---|---|---|---|
| | $(\beta,\gamma)$ | $E_{\rm x}(E_{\rm tot})$ | $(\beta,\gamma)$ | $E_{\rm x}(E_{\rm tot})$ | $I^\pi$ | $E_{\rm x}$ |
| A | (0.28,24.7°) | (-898.09) | (0.28,24.9°) | (-898.14) | $\frac{7}{2}^+$ | |
| E | (0.25,23.1°) | 0.69(-897.40) | (0.25,23.3°) | 0.37(-897.76) | $\frac{15}{2}^-$ | 2.417 |
| F | (0.28,21.8°) | 1.69(-896.40) | (0.28,22.1°) | 1.43(-896.70) | $\frac{23}{2}^+$ | 2.982 |

energies $E_{\rm tot}$, and the excitation energies $E_{\rm x}$ for states E and F with and without time-odd fields are given and compared with the experimental bandhead energies of two rotational bands. The effects of the time-odd fields on the triaxial deformation parameters $\beta, \gamma$ are negligible. Their contribution for the total energy are respectively $-0.05$ MeV for state A, $-0.3$ MeV for state E and $-0.36$ MeV for state F.

The experimental spin, parity and excitation energies of bandheads for two rotational bands based on the configurations of E and F are $\frac{15}{2}^-$, 2.417 MeV and $\frac{23}{2}^+$, 2.982 MeV respectively. It can be seen that the displacement for the energies of two bandheads (0.57 MeV) has been reasonable reproduced by the RMF calculations (1.0 and 1.06 MeV).

It is necessary to note here that in $^{105}$Rh, the suggested configuration $\pi 1g_{9/2}^{-1} \otimes \nu 1h_{11/2}^{1}(1g_{7/2}, 2d_{5/2})^1$ for the candidate chiral doublet bands (band 7 and 8 in Ref. [23]) involves the orbits of pseudospin doublet states $(1g_{7/2}, 2d_{5/2})$. So a competing interpretation of band 7 and 8 includes the pseudospin doublet bands [3]. Further efforts are needed to address this point.

In summary, adiabatic and configuration-fixed constrained triaxial RMF approaches have been applied to investigate the M$\chi$D candidate nucleus $^{105}$Rh. According to the suggested high-$j$ proton hole and high-$j$ neutron particle configurations, their triaxial deformations favorable for the construction of the chiral doublet bands are obtained from the configuration-fixed constrained triaxial RMF calculations. The existence of M$\chi$D phenomenon is expected in $^{105}$Rh. Future efforts should be made to investigate whether the rotating mean field will attain chirality or not.

**Acknowledgments**

This work is partly supported by Major State Basic Research Developing Program 2007CB815000 and the National Natural Science Foundation of China under Grant Nos. 10975007, 10975008 and 110050691.

---

[1] S. Frauendorf and J. Meng, Nucl. Phys. A **617**, 131 (1997).

[2] K. Starosta et al., Phys. Rev. Lett. **86**, 971 (2001).

[3] J. Meng and S. Q. Zhang, J. Phys. G: Nucl. Part. Phys. **37**, 064025 (2010).

[4] J. Meng, S. Q. Zhang, B. Qi, and S. Y. Wang, J. Phys. Conf. Ser. **205**, 012030 (2010).

[5] V. Dimitrov, S. Frauendorf, and F. Donau, Phys. Rev. Lett. **84**, 5732 (2000).

[6] P. Olbratowski, J. Dobaczewski, J. Dudek, and W. Plociennik, Phys. Rev. Lett. **93**, 052501 (2004).

[7] P. Olbratowski, J. Dobaczewski, and J. Dudek, Phys. Rev. C **73**, 054308 (2006).

[8] J. Peng, J. Meng and S. Q. Zhang, Phys. Rev. C **68**, 044324 (2003).

[9] T. Koike, K.Starosta, and I. Hamamoto, Phys. Rev. Lett. **93**, 172502 (2004).

[10] S. Y. Wang, S. Q. Zhang, B. Qi, and J. Meng, Phys. Rev. C **75**, 024309 (2007).

[11] S. Q. Zhang, B. Qi, S. Y. Wang, and J. Meng, Phys. Rev. C **75**, 044307 (2007).

[12] B. Qi *et al.*, Phys. Lett. B **675**, 175 (2009).

[13] P. Ring, Prog. Part. Nucl. Phys. **37**, 193 (1996).

[14] D. Vretenar, A. V. Afanasjev, G. A. Lalazissis, and P. Ring, Phys. Rep. **409**, 101 (2005).

[15] J. Meng *et al.*, Prog. Part. Nucl. Phys. **57**, 470 (2006).

[16] W. Koepf and P. Ring, Nucl. Phys. A **493**, 61 (1989).

[17] A. V. Afanasjev, P. Ring, and J. König, Nucl. Phys. A **676**, 196 (2000).

[18] H. Madokoro, J. Meng, M. Matsuzaki, and S. Yamaji, Phys. Rev. C **62**, 061301 (2000).

[19] J. Peng, J. Meng, P. Ring, and S. Q. Zhang, Phys. Rev. C **78**, 024313 (2008).

[20] J. Meng, J. Peng, S. Q. Zhang, and S.-G. Zhou, Phys. Rev. C **73**, 037303 (2006).

[21] J. Peng *et al.*, Phys. Rev. C **77**, 024309 (2008)

[22] J. M. Yao *et al.*, Phys. Rev. C **79**, 067302 (2009).

[23] J. A. Alcántara-Núñez *et al.*, Phys. Rev. C **69**, 024317 (2004).

[24] J. Timár *et al.*, Phys. Lett. B **598**, 178 (2004).

[25] J. M. Yao, H. Chen, and J. Meng, Phys. Rev. C **74**, 024307 (2006).

[26] J. Li, Y. Zhang, J. M. Yao, and J. Meng, Sci. China Ser. G: Phys. Mech. Astron. **52**, 1586 (2009).

[27] R. Bengtsson, W. Nazarewicz, Z. Phys. A **334**, 269 (1989).

[28] Z. P. Li, T. Niǩsić, D. Vretenar, and J. Meng, Phys. Rev. C **81**, 034316 (2010).

[29] W. Long, J. Meng, N. Van Giai, and S.-G. Zhou, Phys. Rev. C **69**, 034319 (2004).

[30] P. Zhao, B. Sun, and J. Meng, Chin. Phys. Lett. **26**, 112102 (2009).

[31] B. Qi, S. Q. Zhang, S. Y. Wang, J. Meng and T. Koike, Phys. Rev. C 83, 034303 (2011).